Article

Current Biology

Nucleus accumbens neurons expressing dopamine D1 receptors modulate states of consciousness in sevoflurane anesthesia

Highlights

- Chemogenetic activation of NAc^{D1R} neurons delays induction of sevoflurane anesthesia
- Photostimulation of NAc^{D1R} neurons induces cortical activation during anesthesia
- Brief activation of NAc^{D1R} neurons induces behavioral emergence during anesthesia
- NAc^{D1R} neuron inhibition accelerates sevoflurane induction and prolongs emergence

Authors

Wei-Wei Bao, Wei Xu, Gao-Jie Pan, ..., Wei-Min Qu, Wen-Xian Li, Zhi-Li Huang

Correspondence

huangzl@fudan.edu.cn (Z.-L.H.), wenxianli66@gmail.com (W.-X.L.)

In brief

Bao et al. show that nucleus accumbens (NAc) dopamine D1 receptor (D1R)-expressing neurons, when activated, delay sevoflurane induction and induce cortical activation and behavioral emergence during anesthesia. NAc^{D1R} neuron inhibition accelerates induction and prolongs emergence. NAc^{D1R} neuron is a potential target for modulating consciousness.

Bao et al., 2021, Current Biology *31*, 1893–1902
May 10, 2021
https://doi.org/10.1016/j.cub.2021.02.011

CellPress

Current Biology

CellPress

Article

Nucleus accumbens neurons expressing dopamine D1 receptors modulate states of consciousness in sevoflurane anesthesia

Wei-Wei Bao,[1,2,3] Wei Xu,[1,2,3] Gao-Jie Pan,[1] Tian-Xiao Wang,[2] Yuan Han,[1] Wei-Min Qu,[2] Wen-Xian Li,[1,2,*] and Zhi-Li Huang[1,2,4,*]

[1]Department of Anesthesiology, Eye & ENT Hospital, State Key Laboratory of Medical Neurobiology and MOE Frontiers Center for Brain Science, Institutes of Brain Science, Shanghai Medical College, Fudan University, Shanghai 200032, China

[2]Department of Pharmacology, School of Basic Medical Sciences, Shanghai Medical College, Fudan University, Shanghai 200032, China

[3]These authors contributed equally

[4]Lead contact

*Correspondence: wenxianli66@gmail.com (W.-X.L.), huangzl@fudan.edu.cn (Z.-L.H.)

https://doi.org/10.1016/j.cub.2021.02.011

SUMMARY

Although general anesthesia (GA) enables patients to undergo surgery without consciousness, the precise neural mechanisms underlying this phenomenon have yet to be identified. In addition to many studies over the past two decades implicating the thalamus, cortex, brainstem, and conventional sleep-wake circuits in GA-induced loss of consciousness (LOC), some recent studies have begun to highlight the importance of other brain areas as well. Here, we found that population activities of neurons expressing dopamine D1 receptor (D1R) in the nucleus accumbens (NAc), a critical interface between the basal ganglia and limbic system, began to decrease before sevoflurane-induced LOC and gradually returned after recovery of consciousness (ROC). Chemogenetic activation of NAc^{D1R} neurons delayed induction of and accelerated emergence from sevoflurane GA, whereas chemogenetic inhibition of NAc^{D1R} neurons exerted opposite effects. Moreover, transient activation of NAc^{D1R} neurons induced significant cortical activation and behavioral emergence during continuous steady-state GA with sevoflurane or deep anesthesia state with constant and stable burst-suppression oscillations. Taken together, our findings uncover that NAc^{D1R} neurons modulated states of consciousness associated with sevoflurane GA and may represent an area for targeting GA-induced changes in consciousness and ameliorating related adverse effects.

INTRODUCTION

Inhaled anesthetics were first used >170 years ago and have tremendous significance for modern medicine.[1,2] Inhalational general anesthesia (GA) enables patients to undergo surgery without consciousness, pain, or memories of the operations.[3] However, despite decades of scientific research on this phenomenon, the precise neural mechanisms of inhalational GA-induced altered states of consciousness remain unclear.[4,5]

The nucleus accumbens (NAc), a major structure of the ventral striatum, is traditionally involved in behaviors that are critically dependent on heightened arousal, such as motivation, reward, and movement.[6–9] Loss of consciousness (LOC) and recovery of consciousness (ROC) from GA are accompanied by cessation and regaining of these arousal-based behaviors, respectively, suggesting a close relationship between the NAc and GA-induced changes in consciousness. Recent studies have also indicated that the NAc directly participates in sleep-wake regulation.[10–13] However, whether the NAc participates in regulating states of consciousness in GA remains largely unknown. Notably, a few recent laboratory and clinical studies have begun to highlight the importance of the basal ganglia and limbic system in the mechanisms of action of GA;[3,14,15] interestingly, the NAc acts as an important interface between these two systems.[16,17] Recent neuroimaging evidence has also suggested that the NAc may be essential for modulating anesthetic-induced unconsciousness.[18] Additionally, NAc neurons are anatomically connected with numerous brain sites that have been reported to promote reanimation from inhaled GA, such as the ventral tegmental area (VTA),[19,20] paraventricular thalamus (PVT),[21] parabrachial nucleus (PB),[22,23] and prefrontal cortex.[17] Collectively, these results suggest that the NAc may play a key role in regulating states of consciousness in GA.

To test this hypothesis, in the present study, we tested the effects of sevoflurane in mice, as this specific general anesthetic is widely used in clinical settings. We found that population activities of NAc dopamine D1 receptor (D1R)-expressing neurons decreased before LOC in the induction phase and gradually returned after ROC in the emergence phase of sevoflurane GA, as determined via a combination of *in vivo* fiber photometry and polysomnographic recordings. Based on bidirectional chemogenetic experiments, we demonstrated that NAc^{D1R} neurons were sufficient and necessary for modulating anesthetic state transitions with sevoflurane. Finally, transient optogenetic stimulation of NAc^{D1R} neurons robustly induced cortical activation and

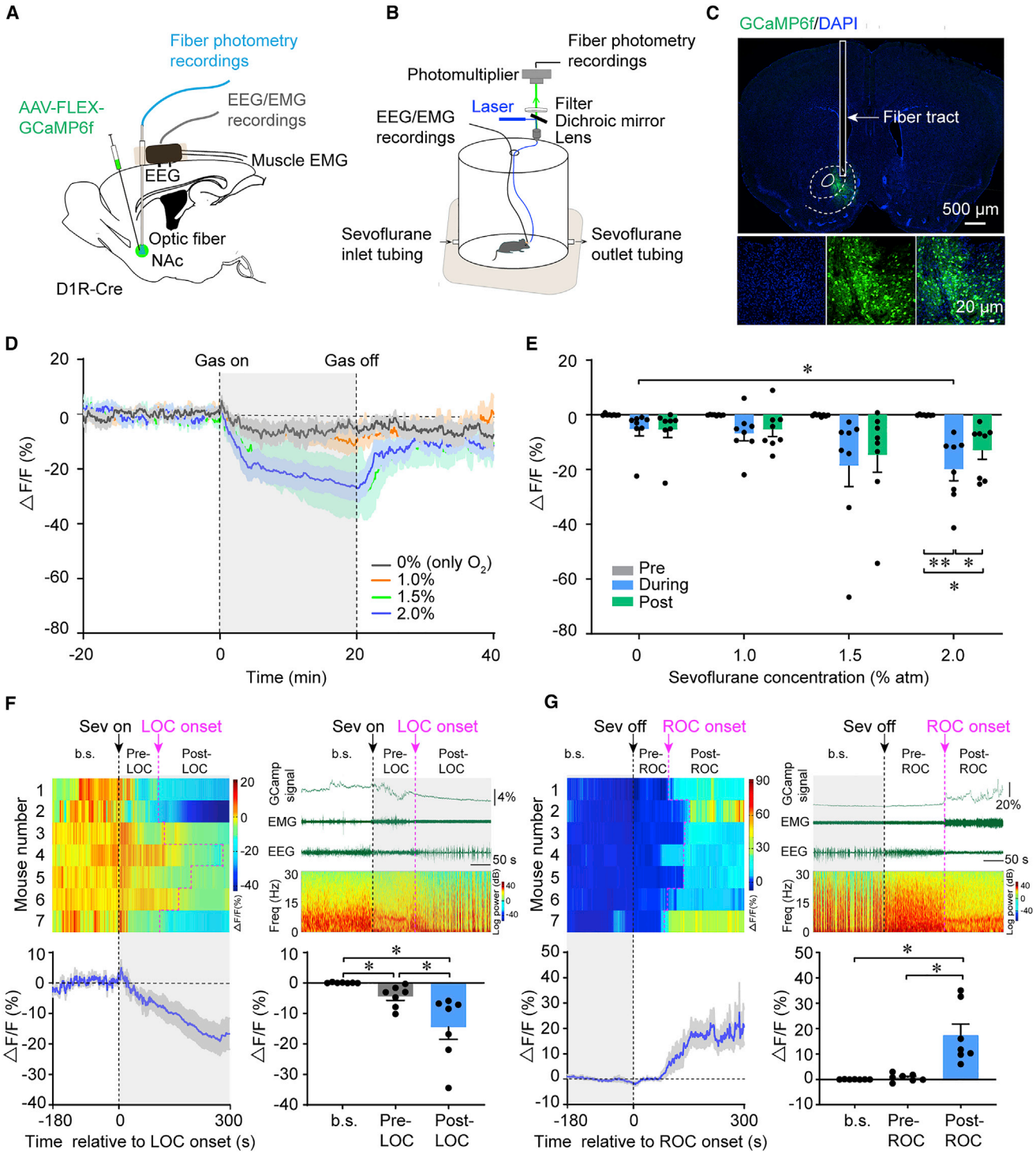

Figure 1. Population activities of NAc^{D1R} neurons in response to sevoflurane GA in mice

(A) Schematic of AAV2/9-hSyn-FLEX-GCaMP6f injected into the NAc of D1R-Cre mice.

(B) Schematic of the recording configuration.

(C) Top: GCaMP6f/DAPI immunofluorescence in NAc^{D1R} neurons and track of the optic fiber implanted above the NAc; scale bar, 500 μm. Bottom: magnified images are shown; scale bar, 20 μm.

(D and E) Time courses of Ca^{2+} signals following sevoflurane anesthesia (D) and quantification of Ca^{2+} signal changes before, during, and after sevoflurane inhalation (E). n = 8 mice for each group.

(legend continued on next page)

behavioral emergence during the sevoflurane maintenance phase or deep anesthesia states with burst-suppression oscillations. Hence, our findings uncover a vital but previously neglected brain site that potently modulates states of consciousness in sevoflurane GA.

RESULTS

Population activities of NAc^{D1R} neurons in response to sevoflurane anesthesia in mice

To investigate whether population activities of NAc^{D1R} neurons correlate with sevoflurane anesthesia, we injected the adeno-associated virus (AAV), AAV-hSyn-FLEX-GCaMP6f, into the NAc of D1R-Cre mice (Figures 1A–1C). As shown in Figures 1D and 1E, in the 0% sevoflurane condition, there was no statistically significant drop in Ca^{2+} signal intensity during the exposure to pure oxygen. Compared with those during the oxygen condition, Ca^{2+} signals of NAc^{D1R} neurons decreased under 2% sevoflurane exposure (2.0% versus 0% sevoflurane: −14.73% ± 4.10%; p = 0.035). However, there was no statistical difference in the Ca^{2+} signals of NAc^{D1R} neurons between 0% and 1% or 1.5% sevoflurane exposure (1.0% versus 0% sevoflurane: −1.56% ± 4.89%, p = 0.988; 1.5% versus 0% sevoflurane: −13.41% ± 8.49%, p = 0.446). Compared with the awake baseline, population activities of NAc^{D1R} neurons were highly suppressed after 2% sevoflurane exposure for 20 min (during versus pre: −19.81% ± 4.18%; p = 0.005) and gradually returned during the recovery period (post versus during: 6.98% ± 1.79%; p = 0.014).

We next analyzed the real-time activities of NAc^{D1R} neurons during induction and emergence phases of 2% sevoflurane GA. For the induction period, we calculated the Ca^{2+} signals in three consecutive time sections (from −180 to 300 s; 0 s was the time point of 2% sevoflurane turning on): −180 to 0 s (pre-anesthesia baseline); the early period of anesthesia before LOC (pre-LOC, from 0 s to LOC); and the initial period after LOC (post-LOC, from LOC to 300 s). Neuronal activities began to decrease during the early period of anesthesia before LOC (pre-LOC versus pre-anesthesia baseline, −4.46% ± 1.38%; p = 0.041; Figure 1F). After LOC, neuronal activities further declined compared with the pre-anesthesia baseline (post-LOC versus pre-anesthesia baseline, −14.56% ± 4.08%; p = 0.028) or the early period of anesthesia before LOC (post-LOC versus pre-LOC, −10.10% ± 2.77%; p = 0.025; Figure 1F). For the emergence period, we analyzed the Ca^{2+} signals in three consecutive time sections (from −180 to 300 s; 0 s was the time point of 2% sevoflurane turning off): −180 to 0 s (unconsciousness anesthesia baseline); pre-return of consciousness (pre-ROC, from 0 s to ROC); and the initial period after ROC (post-ROC, from ROC to 300 s). Compared with the anesthesia baseline, Ca^{2+} signals did not change in the period of pre-ROC (pre-ROC versus anesthesia baseline, 0.69% ± 0.56%; p = 0.478; Figure 1G) but showed a robust increase during the initial period after ROC (post-ROC versus anesthesia baseline, 17.37% ± 4.41%, p = 0.018; post-ROC versus pre-ROC, 16.68% ± 4.46%, p = 0.022; Figure 1G). Collectively, these findings indicate that NAc^{D1R} neurons changed their population activities across different stages of sevoflurane GA.

Chemogenetic activation of NAc^{D1R} neurons delays induction of and accelerates emergence from sevoflurane GA

To explore the casual role of NAc^{D1R} neurons during sevoflurane GA, we chemogenetically activated NAc^{D1R} neurons of D1R-Cre mice with AAV-DIO-hM3Dq-mCherry (Figure 2A). The maximum overlay of hM3Dq expression in the NAc is shown by heatmaps in Figure 2A. Whole-cell recordings of hM3Dq-positive NAc^{D1R} neurons from acute brain slices showed depolarization and firing responses with 5 μM clozapine-N-oxide (CNO) treatment, which confirmed that CNO potently activated hM3Dq-positive NAc^{D1R} neurons (Figure 2B). c-Fos protein was intensively expressed in hM3Dq-positive NAc^{D1R} neurons after CNO injection, whereas vehicle injection induced comparatively little c-Fos expression, suggesting that NAc^{D1R} neurons were robustly activated via the hM3Dq ligand, CNO, *in vivo* (Figure 2C). We further investigated the behavioral consequences of NAc^{D1R} neuronal activation on sevoflurane sensitivity, induction, and emergence via the righting reflex test. Importantly, the loss of righting reflex (LORR) is considered as a surrogate for LOC in humans.[24] Upon administration of CNO to activate NAc^{D1R} neurons, mice required higher doses of sevoflurane to display LORR compared to those of the vehicle group (n = 11; p = 0.006), and the dose-response curve was right shifted (Figure 2D). The minimum alveolar concentration of sevoflurane at which half the mice lost their righting reflex (MAC_{LORR}), also known as the 50% effective concentration (EC_{50}) of sevoflurane on LORR, was 1.42% (95% confidence index [CI] 1.38%–1.46%) for the vehicle group and 1.57% (95% CI 1.54%–1.60%) for the CNO group in hM3Dq mice (Table S1). When exposed to 2% sevoflurane, pretreatment with CNO for 1 h before righting-reflex detection significantly delayed the induction time from 135 ± 6 s to 178 ± 15 s (n = 11; p = 0.005) and accelerated the emergence time from 191 ± 36 s to 123 ± 28 s (n = 10; p = 0.010; Figures 2E and 2F). To rule out any off-target effects of CNO administration at 3 mg/kg, we injected D1R-Cre mice with the control AAV, AAV-DIO-mCherry. Relative to the vehicle, CNO at 3 mg/kg administration did not alter induction of or emergence from sevoflurane GA in mCherry mice (Figure S2). These findings demonstrate that selective activation of NAc^{D1R} neurons reduced sevoflurane sensitivity, as well as delayed induction of and facilitated reanimation from sevoflurane GA.

(F) Left: heatmaps (top) and mean GCaMP6f traces (bottom) ± SEM (shaded area) for NAc^{D1R} neurons during LOC induced by 2% sevoflurane. Top right: example traces of Ca^{2+} signals aligned to LOC state transitions are shown. Bottom right: quantification of Ca^{2+} signal changes in three consecutive time sections is shown. 0 represents the moment of LOC. n = 7 mice.

(G) Left: heatmaps (top) and mean GCaMP6f traces (bottom) ± SEM (shaded area) for NAc^{D1R} neurons during ROC after 2% sevoflurane exposing. Top right: example traces of Ca^{2+} signals aligned to ROC state transitions are shown. Bottom right: quantification of Ca^{2+} signal changes in three consecutive time sections is shown. 0 represents the moment of ROC. n = 7 mice.

The asterisk in (E)–(G) indicates a significant difference (*p < 0.05; **p < 0.01). Statistical comparisons were conducted using one-way (F and G) or two-way (E) repeated-measures ANOVA followed by Tukey's post hoc test. Error bars represent ± SEM. b.s., baseline; Freq, frequency; LOC, loss of consciousness; ROC, recovery of consciousness; Sev, sevoflurane. See also Figure S1.

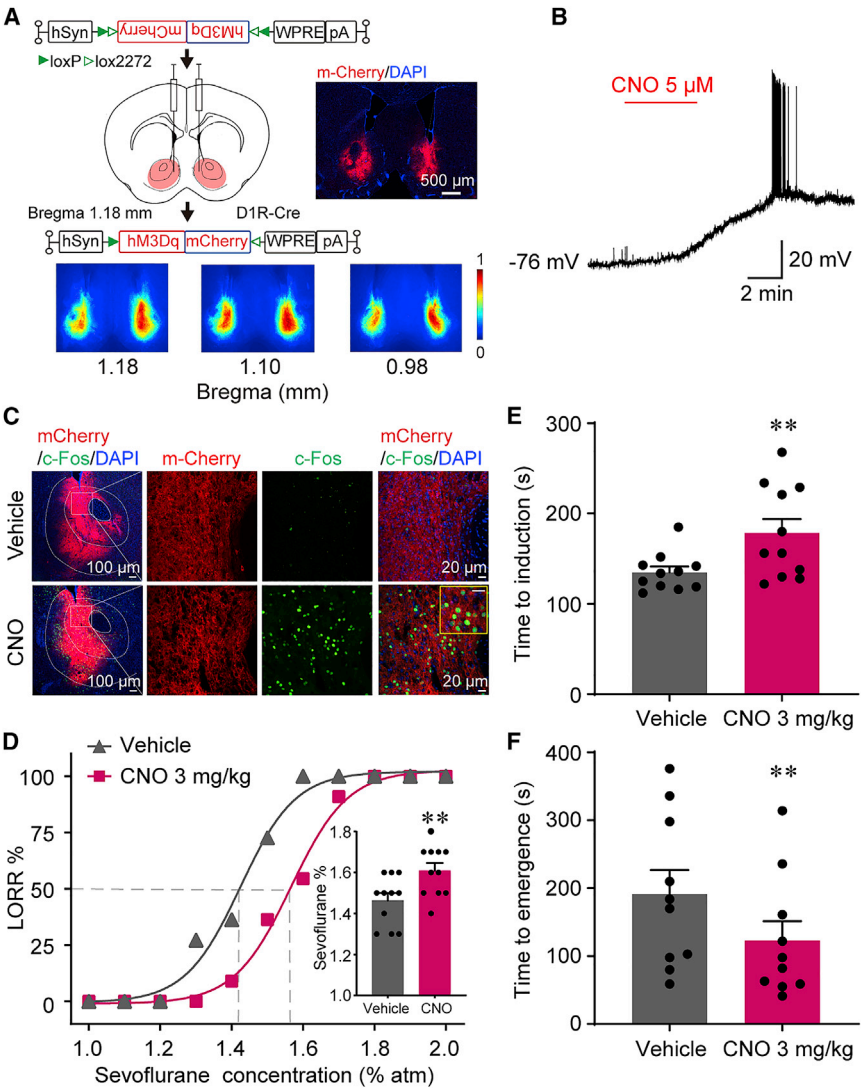

Figure 2. Chemogenetic activation of NAc^{D1R} neurons delays induction of and accelerates emergence from sevoflurane GA

(A) Top: schematic of AAV2/9-hSyn-DIO-hM3D(Gq)-mCherry injected into the NAc of D1R-Cre mice and representative immunohistochemical staining (scale bar, 500 μm). Bottom: heatmaps show overlay of hM3Dq expression in the NAc (bregma 0.98–1.18 mm) of all injected mice: "1," the area of maximum overlap (red color); "0," the area of minimum overlap (blue color).

(B) Bath application of CNO (5 μM) increased firing rate in hM3Dq-positive NAc^{D1R} neurons *in vitro*.

(C) Left: representative images of mCherry/c-Fos/DAPI immunofluorescence in NAc^{D1R} neurons after vehicle or CNO treatment; scale bar, 100 μm. Right: magnified images are shown; scale bar, 20 μm.

(D) Dose-response curves showing the percentages of mice exhibiting LORR in response to incremental sevoflurane concentrations for the vehicle group and the CNO group. Inset: the sevoflurane concentrations at which each mouse exhibited LORR are shown (n = 11).

(E) Induction time with 2% sevoflurane exposure after intraperitoneal (i.p.) injections of vehicle or CNO for 1 h (n = 11).

(F) Emergence time with 2% sevoflurane exposure for 1 h after i.p. injections of vehicle or CNO (n = 10). The asterisk in (D)–(F) indicates a significant difference (**p < 0.01). Statistical comparisons were conducted using Wilcoxon signed-rank test (D) or Student's two-tailed paired t test (E and F). Error bars represent ± SEM. CNO, clozapine-N-oxide; LORR, loss of righting reflex. See also Table S1.

Chemogenetic inhibition of NAc^{D1R} neurons facilitates induction of and prolongs emergence from sevoflurane GA

To further explore the behavioral consequences of chemogenetic inhibition of NAc^{D1R} neurons, AAV-DIO-hM4Di-mCherry was injected into the NAc of D1R-Cre mice to inhibit NAc^{D1R} neurons. Heatmaps in Figure 3A represent the maximum overlap of hM4Di expression in the NAc (bregma 0.98–1.18 mm). Whole-cell recordings of hM4Di-positive NAc^{D1R} neurons from acute brain slices showed a decreased number of evoked action potentials with CNO, implying that CNO was sufficient to inhibit hM4Di-positive D1R neurons in the NAc (Figure 3B). Furthermore, there was almost no c-Fos expression in the NAc after CNO treatment compared with that in the vehicle group (Figure 3C). Compared with those in the vehicle group, the dose-response curve for LORR in the CNO group was left shifted, and the MAC_{LORR} was reduced from 1.38% (95% CI 1.37%–1.38%) to 1.14% (95% CI 0.95%–1.18%; Figure 3D; Table S1), suggesting that animals were more sensitive to sevoflurane after inhibition of NAc^{D1R} neurons (n = 10; p = 0.001). When exposed to 2% sevoflurane, systemic CNO treatment significantly accelerated the induction time from 117 ± 6 s to 79 ± 5 s (n = 8; p = 0.004) and prolonged the emergence time from 107 ± 11 s to 296 ± 58 s (n = 12; p = 0.006; Figures 3E and 3F). Taken together, these results indicate that selective inhibition of D1R neurons in the NAc increased sevoflurane sensitivity, accelerated induction, and delayed emergence from sevoflurane GA.

Optogenetic stimulation of NAc^{D1R} neurons induces cortical activation and behavioral emergence during continuous steady-state GA with sevoflurane

To test whether activation of NAc^{D1R} neurons is sufficient to restore states of consciousness during the sevoflurane maintenance phase, we injected AAV-DIO-ChR2-mCherry or AAV-DIO-mCherry into the NAc of D1R-Cre mice (Figure 4A). Functional expression of ChR2 was confirmed by whole-cell patch-clamp recordings (Figure 4B). We applied acute optical stimulation (lasting 60 s) after mice maintained LORR for 20 min during continuous steady-state general anesthesia (CSSGA) with sevoflurane. Photostimulation (10–30 Hz, 5 ms, 60 s) of NAc^{D1R} neurons under sevoflurane CSSGA reliably induced behavioral emergence in a frequency-dependent manner (Figure 4C), with the highest proportion in regaining righting reflex at 30 Hz (Figure 4D). Laser

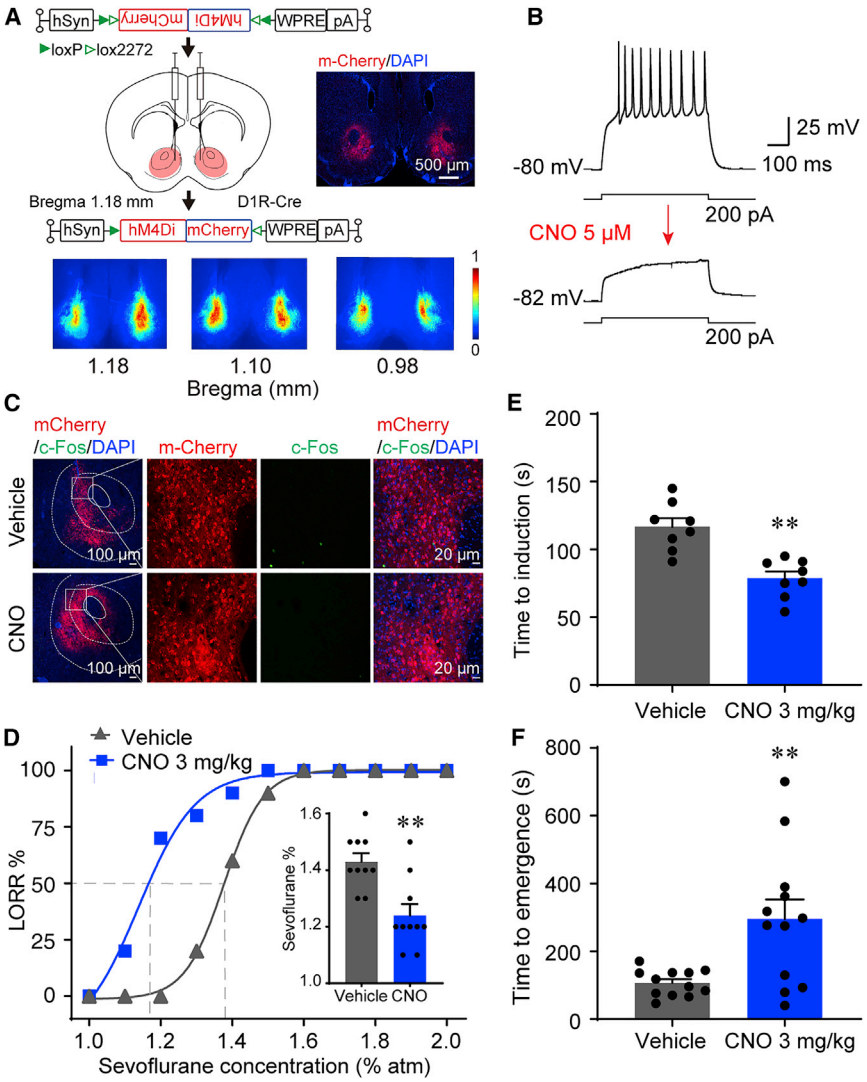

Figure 3. Chemogenetic inhibition of NAc^{D1R} neurons facilitates induction of and prolongs emergence from sevoflurane GA

(A) Top: schematic of AAV2/9-hSyn-DIO-hM4D(Gi)-mCherry injected into the NAc of D1R-Cre mice and representative immunohistochemical staining (scale bar, 500 μm). Bottom: heatmaps show overlay of hM4Di expression in the NAc (bregma 0.98–1.18 mm) of all injected mice: 1, the area of maximum overlap (red color); 0, the area of minimum overlap (blue color).

(B) Bath application of CNO (5 μM) reduced firing rate of hM4Di-positive NAc^{D1R} neurons injected with 200 pA current *in vitro*.

(C) Left: representative images of mCherry/c-Fos/DAPI immunofluorescence in the NAc after vehicle or CNO treatment; scale bar, 100 μm. Right: magnified images are shown; scale bar, 20 μm.

(D) Dose-response curves showing the percentages of mice exhibiting LORR in response to incremental sevoflurane concentrations after injection of vehicle or CNO. Inset: the sevoflurane concentrations at which each mouse showed LORR are shown (n = 10).

(E) Induction time with 2% sevoflurane exposure after i.p. injections of vehicle or CNO for 1 h (n = 8).

(F) Emergence time with 2% sevoflurane exposure for 1 h after i.p. injections of vehicle or CNO (n = 12). The asterisk in (D)–(F) indicates a significant difference (**p < 0.01). Statistical comparisons were conducted using Student's two-tailed paired t test (D–F). Error bars represent ± SEM. See also Table S1.

activation of NAc^{D1R} neurons in ChR2 mice at 30 Hz induced obvious behavioral emergence, including body movements (i.e., of the limbs, head, and tail; 9/9), righting (6/9), and walking (5/9) in ChR2 mice (Table S2). However, mCherry mice exhibited no obvious behavioral responses during photostimulation (Figure 4C; Table S2; Video S2). The Bayesian 95% CI for the difference in the probability of righting (walking) at 30 Hz between the two groups was 0.158–0.818 (0.069–0.748; Figure 4E). The posterior probability of the difference in righting (walking) between the two groups greater than 0 at 30 Hz was 0.9962 (0.9887), which was statistically significant (Figure 4F). In addition, photostimulation of NAc^{D1R} neurons at 30 Hz rapidly induced a brain-state transition from slow-wave activity or a burst-suppression pattern to low-voltage fast activity in ChR2 mice (Figure 4G; Video S1), but not in mCherry mice (Figure 4J; Video S2). Spectral analysis of electroencephalogram (EEG) data revealed that acute photostimulation of NAc^{D1R} neurons at 30 Hz induced a significant decrease in delta power (44.62% ± 3.94% versus 35.88% ± 1.93%; p < 0.001) and an increase in beta power (8.08% ± 0.80% versus 13.84% ± 1.20%; p = 0.025; Figure 4I). To further illustrate these changes, corresponding EEG power densities are also presented in Figure 4H. Photostimulation of NAc^{D1R} neurons at 20 Hz was still sufficient to cause a significant change, as reflected by arousal scores and spectral analysis (Figures 4C and S3A). However, no differences were observed in mCherry mice (Figures 4K, 4L, S3B, and S3D). These findings indicate that optogenetic activation of NAc^{D1R} neurons was sufficient to induce cortical activation and behavioral emergence during sevoflurane maintenance.

Optogenetic stimulation of NAc^{D1R} neurons induces cortical activation and behavioral emergence during burst-suppression oscillations induced by deep sevoflurane anesthesia

We further investigated the effects of NAc^{D1R} neuronal activation on states of consciousness during constant and stable burst-suppression oscillations, which are usually observed under deep states of GA. We activated NAc^{D1R} neurons *in vivo* with 5-ms pulses of blue light at 10–30 Hz for 30 s, when a stable EEG burst-suppression mode (lasting at least for 5 min) was observed during sevoflurane maintenance. Acute photostimulation of NAc^{D1R} neurons at 30 Hz induced ~100% cortical activation, and some ChR2 mice displayed wake-like behaviors as defined by increased electromyogram (EMG) activities or slight body

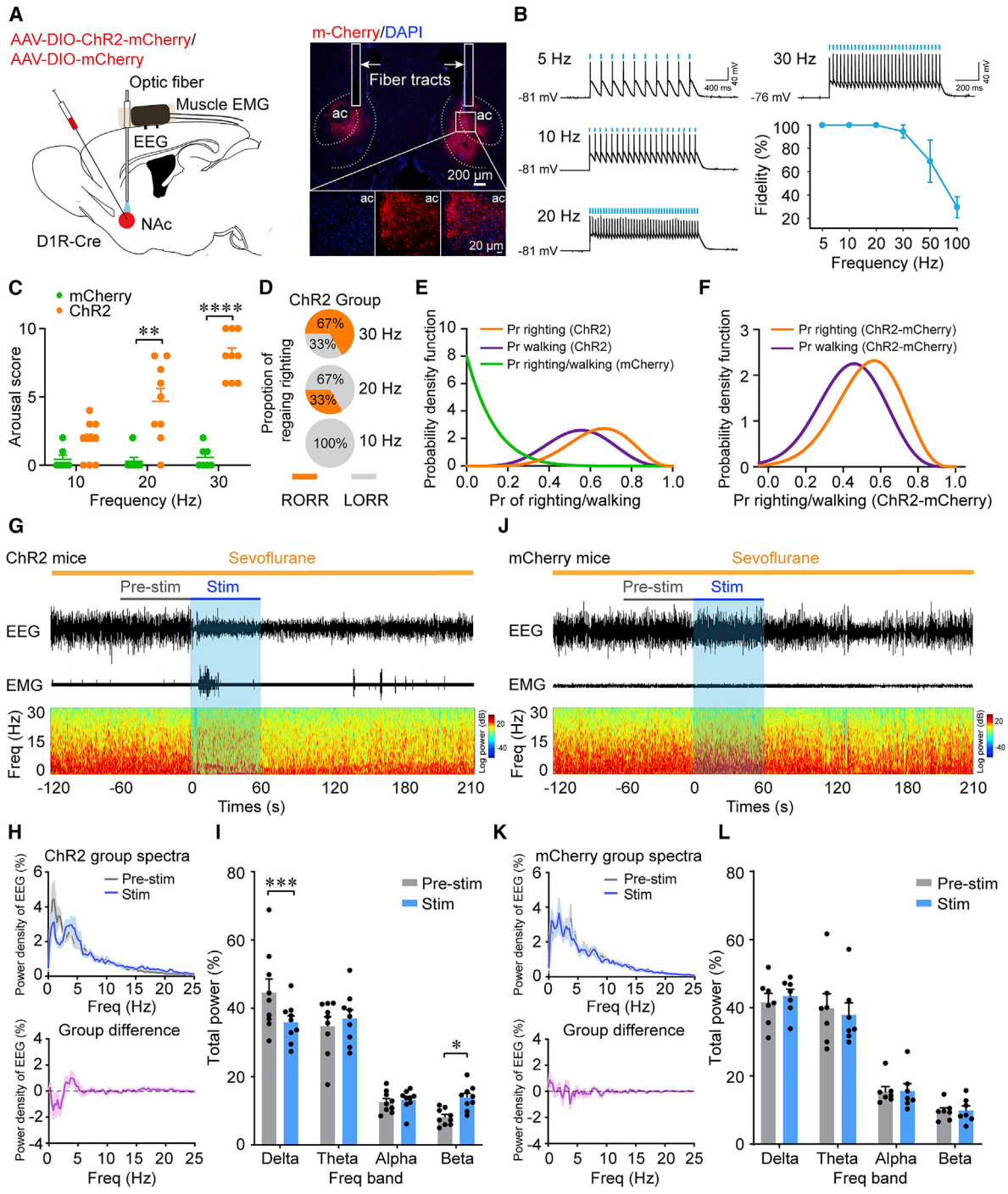

Figure 4. Optogenetic stimulation of NAc^{D1R} neurons induces cortical activation and behavioral emergence during continuous steady-state GA with sevoflurane

(A) Left: schematic showing injection of AAV2/9-EF1α-DIO-ChR2-mCherry or AAV2/9-EF1α-DIO-mCherry into the NAc of D1R-Cre mice. Right: representative images of mCherry/DAPI immunofluorescence in the NAc (scale bar, 200 μm) and magnified images (scale bar, 20 μm) are shown.

(B) Representative traces and fidelity of neuronal firing in ChR2-expressing NAc^{D1R} neurons evoked by 473-nm light stimulation at different frequencies.

(C) Arousal scores based on behavioral responses of mice under sevoflurane CSSGA during photostimulation of NAc^{D1R} neurons (10–30 Hz, 5 ms, 60 s). n = 9 ChR2 mice or n = 7 mCherry mice per group.

(D) Pie charts showing the proportion of ChR2 mice regaining their righting reflex following photostimulation of NAc^{D1R} neurons at 10–30 Hz for 60 s. n = 9 ChR2 mice per group.

(E) Posterior densities for the probabilities of righting and walking for the ChR2 (n = 9) group and mCherry (n = 7) group under sevoflurane CSSGA during photostimulation of NAc^{D1R} neurons at 30 Hz for 60 s.

(legend continued on next page)

movements (Figure 5A; Video S3). EEG/EMG activity after photostimulation at 30 Hz mostly shifted from a burst-suppression oscillation mode toward a low-amplitude, high-frequency EEG with increased EMG activity (Figure 5A; Video S3). Interestingly, EEG activation mainly occurred at the later period of photostimulation (average latency ~20 s at 30 Hz), and this change sustained for a few minutes before returning to burst-suppression mode. There was no statistical difference in the burst-suppression ratio (BSR) (41.06% ± 4.14% versus 36.39% ± 4.10%; p = 0.384) between the 30 s before and the 30 s during photostimulation (Figure 5D), but photostimulation still produced a relative decrease in delta power (49.29% ± 1.97% versus 41.49% ± 2.49%; p = 0.037) and an increase in beta power (8.01% ± 0.57% versus 11.67% ± 0.77%; p = 0.016; Figures 5B and 5C). However, ChR2 mice exhibited a robust reduction in BSR during the 30 s after photostimulation compared with the 30 s before (9.87% ± 4.24% versus 41.06% ± 4.14%; p < 0.0001) or the 30 s during (9.87% ± 4.24% versus 36.39% ± 4.10%; p = 0.001) photostimulation (Figure 5D). Moreover, there was an obvious alteration in the normalized EEG power spectrum after photostimulation at 30 Hz (Figure 5B). The total power percentage of the delta power decreased from 49.29% ± 1.97% to 36.98% ± 3.42% (p = 0.026), and the beta power increased from 8.01% ± 0.57% to 14.03% ± 1.54% (p = 0.019; Figure 5C). Photostimulation of NAc^{D1R} neurons at 20 Hz in ChR2 mice also caused a significant reduction in BSR (post-pre comparison, 29.55% ± 4.60% versus 48.79% ± 3.38%, p = 0.014; post-during comparison, 29.55% ± 4.60% versus 43.48% ± 4.56%, p = 0.004; Figure S4C). In contrast, there were no significant changes in mCherry mice with 10–30 Hz photostimulation (Figures 5E–5H, S4D–S4F, and S4J–S4L; Video S4) or in ChR2 mice with 10 Hz photostimulation (Figures S4G–S4I). These findings collectively illustrate that NAc^{D1R} neuronal activation was sufficient to promote cortical activation and behavioral emergence during deep states of sevoflurane GA with burst-suppression oscillations.

DISCUSSION

Here, combining *in vivo* fiber photometry recordings, chemogenetic/optogenetic manipulations, behavioral tests, and polysomnographic recordings, we identified a specific neuronal subpopulation in the ventral striatum that plays a modulatory role during different stages of sevoflurane GA. We showed that the Ca^{2+} signals of NAc^{D1R} neurons began to decrease before LOC during sevoflurane induction and gradually increased after ROC during the emergence phase. Although emergence from GA is not a simple reversal of induction,[4] our present study revealed that induction into and emergence from sevoflurane GA were both significantly affected by neuronal activity of NAc^{D1R} cells, indicating the existence of shared neural circuits in modulating consciousness during the two different stages of GA. Finally, we revealed that activation of NAc^{D1R} neurons effectively induced cortical activation and behavioral emergence during CSSGA or burst-suppression oscillations. To our knowledge, this is the first demonstration of the potency of NAc^{D1R} neurons in mediating states of consciousness associated with GA. Burst suppression has also been observed in several different etiologies, such as coma, cardiac arrest, hypothermia, and hypoxia.[25,26] Our present results, therefore, not only emphasize the modulatory role of NAc^{D1R} neurons in sevoflurane anesthesia but also encourage further work to explore their role in other types of etiologies displaying similar burst-suppression waves. Moreover, given that different anesthetics induce different EEG signatures and have distinct molecular targets,[5,27,28] it is difficult to predict whether NAc^{D1R} neurons modulate consciousness with the use of other anesthetics.

Our experiments revealed some significant conceptual findings. First, cortical and behavioral state transitions under a burst-suppression oscillation mode were much longer than those under CSSGA with lighter sevoflurane or during non-rapid eye movement (NREM) sleep. Our previous work has shown that the transition from slow-wave sleep to wakefulness is immediate after optoactivation of NAc^{D1R} neurons in freely moving mice.[11] Sevoflurane at a burst-suppression concentration has been reported to robustly disrupt intracortical and thalamocortical functional connectivity,[29,30] which may require more time to meet the cortical threshold for restoration of normal network connectivity and brain-state transitions. Another possible explanation is that NAc^{D1R} neurons are modulators of burst suppression and play their role via projections to the downstream ''off switch'' of burst suppression. EEG oscillation modes (e.g., burst-suppression oscillations, delta oscillations, and slow-wave sleep oscillations), brain states (e.g., depth of anesthesia, population activities of specific neurons, and changes in functional connectivity), and different neural mechanisms underlying sleep and GA may all contribute to temporal differences in governing states of consciousness. Second, during deep anesthesia states, cortical EEG activation was sustained for a few minutes even after transient activation of NAc^{D1R} neurons in our present study. This is unexpected because it is in contrast with the effects of glutamatergic neuronal activation in the PB or PVT, as these manipulations do not induce sustained cortical activation after photostimulation is terminated;[21,22] however, this phenomenon has also been observed in the activation of the lateral hypothalamus-^{GABA} (LH^{GABA})–thalamic reticular nucleus circuit.[24] These results

(F) The difference in the probability of righting and walking between the ChR2 (n = 9) group and mCherry (n = 7) group derived from the beta distribution under sevoflurane CSSGA during photostimulation of NAc^{D1R} neurons at 30 Hz for 60 s.
(G) An example showing EEG, EMG, and EEG spectrograms in a ChR2 mouse following acute photostimulation (30 Hz, 5 ms, 60 s) during sevoflurane CSSGA.
(H) Normalized power densities of EEG signals before and during photostimulation at 30 Hz in ChR2 mice (top) and differences between them (bottom), n = 9. Shading indicates SEM.
(I) Relative EEG power before (gray) and during (blue) photostimulation at 30 Hz in ChR2 mice during sevoflurane CSSGA, n = 9.
(J–L) Similar to (G)–(I) but for mCherry mice, n = 7.
The asterisk in (C) and (I) indicates a significant difference (*p < 0.05; **p < 0.01; ***p < 0.001; ****p < 0.0001). Statistical comparisons were conducted using Mann-Whitney rank-sum test for each frequency (C) or two-way repeated-measures ANOVA followed by Sidak's post hoc test (I and L). Error bars represent ± SEM. Pr, probability; RORR, recovery of righting reflex; Stim, stimulation. See also Figures S1 and S3, Table S2, andVideos S1 and S2.

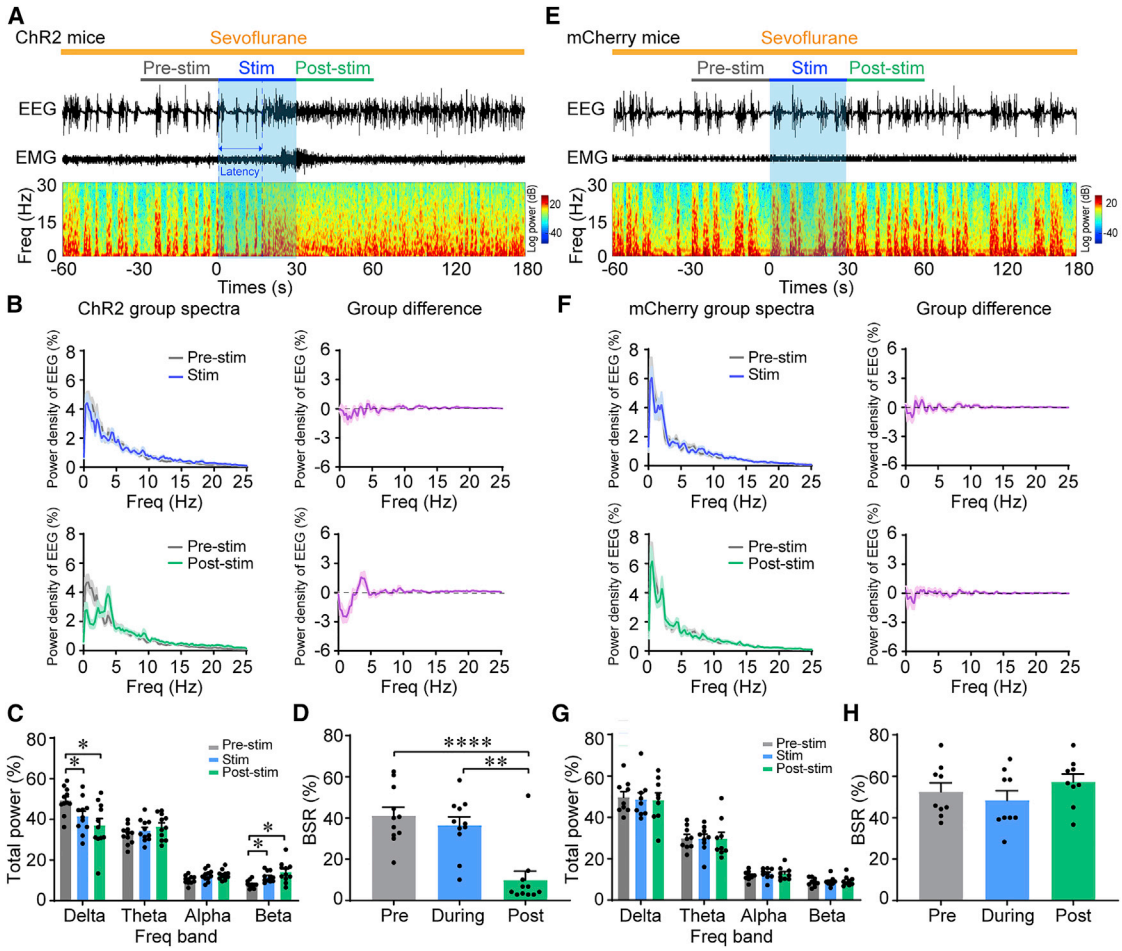

Figure 5. Optogenetic stimulation of NAc^{D1R} neurons induces cortical activation and behavioral emergence during burst-suppression oscillations induced by deep sevoflurane anesthesia

(A) An example showing EEG, EMG, and EEG spectrograms in a ChR2 mouse following acute photostimulation (30 Hz, 5 ms, 30 s) during constant and stable burst-suppression oscillations induced by deep sevoflurane anesthesia.

(B) Top: normalized power densities of EEG signals before and during acute photostimulation at 30 Hz in ChR2 mice (left) and differences between them (right). Bottom: normalized power densities of EEG signals before and after photostimulation at 30 Hz in ChR2 mice (left) and differences between them (right; n = 11 ChR2 mice, 22 trials) are shown. Shading indicates SEM.

(C and D) Relative EEG power (C) and BSR (D) before (gray), during (blue), and after (green) acute photostimulation at 30 Hz in ChR2 mice (n = 11 ChR2 mice, 22 trials).

(E–H) Similar to (A)–(D) but for mCherry mice (n = 9 mCherry mice, 18 trials).

The asterisk in (C and D) indicates a significant difference (*$p < 0.05$; **$p < 0.01$; ****$p < 0.0001$). Statistical comparisons were conducted using one-way (D and H) or two-way (C and G) repeated-measures ANOVA followed by Tukey's post hoc test. Error bars represent ± SEM. BSR, burst-suppression ratio. See also Figures S1 and S4 and Videos S3 and S4.

highlight that the regulation of consciousness and corresponding modulatory effects are highly specific to different brain regions. Furthermore, long-lasting peptidergic signaling has been reported to be vital for regulating GA-induced LOC.[31] NAc^{D1R} neurons may facilitate the release of neuropeptides, and these neuropeptides may further influence multiple neural activities and work on a longer timescale.

Another surprising finding was that NAc^{D1R} neurons induced both cortical activation and behavioral emergence during sevoflurane maintenance. A disassociation between cortical activation and behavioral emergence has been reported in previous studies. For example, microinjection of histamine into the basal forebrain or optoactivation of PVT glutamatergic neurons only shifts the EEG pattern from a burst-suppression pattern to delta activity but fails to induce behavioral responses.[21,32] In contrast, in our present study, photostimulation of NAc^{D1R} neurons effectively changed the EEG pattern from burst-suppression oscillations to low-voltage fast activity and induced behavioral emergence in some mice. Brief activation of NAc^{D1R} neurons during CSSGA induced obvious wake-like behaviors and cortical activation. Activation of VTA dopamine neurons during CSSGA has also been reported to produce a profound behavioral emergence and significant EEG changes (<5 Hz and 6–17 Hz).[19] Taken together, our present findings suggest that NAc^{D1R} neurons are capable of regulating states of consciousness in GA by effectively coordinating brain states and behavioral responses. As a part of the basal ganglia

modulating motivation and movement, NAc^{D1R} neurons may modulate sevoflurane GA-related behavioral emergence through the basal ganglia circuitry. However, in the present study, in most cases, we observed that optoactivation of NAc^{D1R} neurons decreased the EEG amplitudes first, followed by signs of behavioral emergence with increased EMG tone. This time lag indicates the existence of other neural circuits in mediating NAc^{D1R} neuron activation-induced wake-like behavior, such as the downstream wake-promoting LH^{GABA} neurons.[11,24] This phenomenon has also been observed in the transition from NREM sleep to wakefulness.[11]

Recent studies have demonstrated the importance of D1Rs in GA, whereas D1R-binding sites are widely distributed throughout the entire brain.[33,34] Whether D1Rs in other brain areas mediate GA still needs to be further investigated. Moreover, because the NAc is composed of five discernable cell types,[6] further investigations are also needed to uncover the role of other NAc neuronal subpopulations in the mechanism of action of GA and how these subpopulations interact with each other.

In conclusion, our results uncovered a familiar but previously neglected brain site that effectively modulates states of consciousness in sevoflurane GA and offers a potential brain site to target in future studies on GA-induced alterations in consciousness. Therapeutic strategies targeting NAc^{D1R} neurons may help to further elucidate the etiologies of GA-related adverse effects and disorders of consciousness.

STAR★METHODS

Detailed methods are provided in the online version of this paper and include the following:

- KEY RESOURCES TABLE
- RESOURCE AVAILABILITY
  - Lead contact
  - Materials availability
  - Data and code availability
- EXPERIMENTAL MODEL AND SUBJECT DETAILS
  - Mice
- METHOD DETAILS
  - Surgery
  - Fiber photometry recording
  - Chemogenetic manipulations
  - Optogenetic stimulation during burst suppression
  - Optogenetic manipulations during CSSGA
  - EEG/EMG analysis
  - Arousal scoring during CSSGA
  - Immunohistochemistry
  - *In vitro* electrophysiology
- QUANTIFICATION AND STATISTICAL ANALYSIS

SUPPLEMENTAL INFORMATION

Supplemental Information can be found online at https://doi.org/10.1016/j.cub.2021.02.011.

ACKNOWLEDGMENTS

We thank Hui Dong, Ze-Ka Chen, Han Guo, and Pei-Wen Song (Fudan University) for technical assistance. This study was financially supported in part by grants-in-aid for scientific research from the National Natural Science Foundation of China (8202010801, 81671059, 32070984, 31871072, 81671317, and 81971238), Shanghai Municipal Science and Technology Major Project (2018SHZDZX01) and ZJ Lab, Program for Shanghai Outstanding Academic Leaders (to Z.-L.H.), Shanghai Municipal Health and Family Planning Commission Research Project (2018ZHYL0209 and 2019SY015), and Shanghai Science and Technology Committee (17441903000).

AUTHOR CONTRIBUTIONS

W.-W.B. conceived, designed, and performed the experiments, as well as analyzed/interpreted the data, prepared the figures, and wrote the manuscript. W.X. and G.-J.P. performed the experiments, analyzed the data, prepared the figures, and wrote the manuscript. T.-X.W. performed experiments and analyzed data. Y.H. analyzed/interpreted the data and revised the manuscript. W.-M.Q., W.-X.L., and Z.-L.H. conceived and designed the experiments as well as wrote and revised the manuscript.

DECLARATION OF INTERESTS

The authors declare no competing interests.

Received: July 12, 2020
Revised: December 18, 2020
Accepted: February 4, 2021
Published: March 10, 2021

REFERENCES

1. Brown, E.N., Lydic, R., and Schiff, N.D. (2010). General anesthesia, sleep, and coma. N. Engl. J. Med. *363*, 2638–2650.
2. Rudolph, U., and Antkowiak, B. (2004). Molecular and neuronal substrates for general anaesthetics. Nat. Rev. Neurosci. *5*, 709–720.
3. Leung, L.S., Luo, T., Ma, J., and Herrick, I. (2014). Brain areas that influence general anesthesia. Prog. Neurobiol. *122*, 24–44.
4. Kelz, M.B., García, P.S., Mashour, G.A., and Solt, K. (2019). Escape from oblivion: neural mechanisms of emergence from general anesthesia. Anesth. Analg. *128*, 726–736.
5. Hemmings, H.C., Jr., Riegelhaupt, P.M., Kelz, M.B., Solt, K., Eckenhoff, R.G., Orser, B.A., and Goldstein, P.A. (2019). Towards a comprehensive understanding of anesthetic mechanisms of action: a decade of discovery. Trends Pharmacol. Sci. *40*, 464–481.
6. Castro, D.C., and Bruchas, M.R. (2019). A motivational and neuropeptidergic hub: anatomical and functional diversity within the nucleus accumbens shell. Neuron *102*, 529–552.
7. Yang, H., de Jong, J.W., Tak, Y., Peck, J., Bateup, H.S., and Lammel, S. (2018). Nucleus accumbens subnuclei regulate motivated behavior via direct inhibition and disinhibition of VTA dopamine subpopulations. Neuron *97*, 434–449.e4.
8. Russo, S.J., and Nestler, E.J. (2013). The brain reward circuitry in mood disorders. Nat. Rev. Neurosci. *14*, 609–625.
9. Li, Y.D., Luo, Y.J., Xu, W., Ge, J., Cherasse, Y., Wang, Y.Q., Lazarus, M., Qu, W.M., and Huang, Z.L. (2020). Ventral pallidal GABAergic neurons control wakefulness associated with motivation through the ventral tegmental pathway. Mol. Psychiatry. Published online October 14, 2020. https://doi.org/10.1038/s41380-020-00906-0.
10. Oishi, Y., Xu, Q., Wang, L., Zhang, B.J., Takahashi, K., Takata, Y., Luo, Y.J., Cherasse, Y., Schiffmann, S.N., de Kerchove d'Exaerde, A., et al. (2017). Slow-wave sleep is controlled by a subset of nucleus accumbens core neurons in mice. Nat. Commun. *8*, 734.
11. Luo, Y.J., Li, Y.D., Wang, L., Yang, S.R., Yuan, X.S., Wang, J., Cherasse, Y., Lazarus, M., Chen, J.F., Qu, W.M., and Huang, Z.L. (2018). Nucleus accumbens controls wakefulness by a subpopulation of neurons expressing dopamine D_1 receptors. Nat. Commun. *9*, 1576.
12. Lazarus, M., Huang, Z.L., Lu, J., Urade, Y., and Chen, J.F. (2012). How do the basal ganglia regulate sleep-wake behavior? Trends Neurosci. *35*, 723–732.

13. Lazarus, M., Chen, J.F., Urade, Y., and Huang, Z.L. (2013). Role of the basal ganglia in the control of sleep and wakefulness. Curr. Opin. Neurobiol. *23*, 780–785.

14. Huang, Y., Hu, K., Green, A.L., Ma, X., Gillies, M.J., Wang, S., Fitzgerald, J.J., Pan, Y., Martin, S., Huang, P., et al. (2020). Dynamic changes in rhythmic and arrhythmic neural signatures in the subthalamic nucleus induced by anaesthesia and tracheal intubation. Br. J. Anaesth. *125*, 67–76.

15. Crone, J.S., Lutkenhoff, E.S., Bio, B.J., Laureys, S., and Monti, M.M. (2017). Testing proposed neuronal models of effective connectivity within the cortico-basal ganglia-thalamo-cortical loop during loss of consciousness. Cereb. Cortex *27*, 2727–2738.

16. Papp, E., Borhegyi, Z., Tomioka, R., Rockland, K.S., Mody, I., and Freund, T.F. (2012). Glutamatergic input from specific sources influences the nucleus accumbens-ventral pallidum information flow. Brain Struct. Funct. *217*, 37–48.

17. Mhuircheartaigh, R.N., Rosenorn-Lanng, D., Wise, R., Jbabdi, S., Rogers, R., and Tracey, I. (2010). Cortical and subcortical connectivity changes during decreasing levels of consciousness in humans: a functional magnetic resonance imaging study using propofol. J. Neurosci. *30*, 9095–9102.

18. Liang, Z., King, J., and Zhang, N. (2012). Intrinsic organization of the anesthetized brain. J. Neurosci. *32*, 10183–10191.

19. Taylor, N.E., Van Dort, C.J., Kenny, J.D., Pei, J., Guidera, J.A., Vlasov, K.Y., Lee, J.T., Boyden, E.S., Brown, E.N., and Solt, K. (2016). Optogenetic activation of dopamine neurons in the ventral tegmental area induces reanimation from general anesthesia. Proc. Natl. Acad. Sci. USA *113*, 12826–12831.

20. Li, J., Li, H., Wang, D., Guo, Y., Zhang, X., Ran, M., Yang, C., Yang, Q., and Dong, H. (2019). Orexin activated emergence from isoflurane anaesthesia involves excitation of ventral tegmental area dopaminergic neurones in rats. Br. J. Anaesth. *123*, 497–505.

21. Ren, S., Wang, Y., Yue, F., Cheng, X., Dang, R., Qiao, Q., Sun, X., Li, X., Jiang, Q., Yao, J., et al. (2018). The paraventricular thalamus is a critical thalamic area for wakefulness. Science *362*, 429–434.

22. Wang, T.X., Xiong, B., Xu, W., Wei, H.H., Qu, W.M., Hong, Z.Y., and Huang, Z.L. (2019). Activation of parabrachial nucleus glutamatergic neurons accelerates reanimation from sevoflurane anesthesia in mice. Anesthesiology *130*, 106–118.

23. Luo, T., Yu, S., Cai, S., Zhang, Y., Jiao, Y., Yu, T., and Yu, W. (2018). Parabrachial neurons promote behavior and electroencephalographic arousal from general anesthesia. Front. Mol. Neurosci. *11*, 420.

24. Herrera, C.G., Cadavieco, M.C., Jego, S., Ponomarenko, A., Korotkova, T., and Adamantidis, A. (2016). Hypothalamic feedforward inhibition of thalamocortical network controls arousal and consciousness. Nat. Neurosci. *19*, 290–298.

25. Kroeger, D., and Amzica, F. (2007). Hypersensitivity of the anesthesia-induced comatose brain. J. Neurosci. *27*, 10597–10607.

26. Chemali, J., Ching, S., Purdon, P.L., Solt, K., and Brown, E.N. (2013). Burst suppression probability algorithms: state-space methods for tracking EEG burst suppression. J. Neural Eng. *10*, 056017.

27. Solt, K. (2018). Using anesthesia to reveal the elements of consciousness. Trends Cogn. Sci. *22*, 961–962.

28. Akeju, O., and Brown, E.N. (2017). Neural oscillations demonstrate that general anesthesia and sedative states are neurophysiologically distinct from sleep. Curr. Opin. Neurobiol. *44*, 178–185.

29. Ranft, A., Golkowski, D., Kiel, T., Riedl, V., Kohl, P., Rohrer, G., Pientka, J., Berger, S., Thul, A., Maurer, M., et al. (2016). Neural correlates of sevoflurane-induced unconsciousness identified by simultaneous functional magnetic resonance imaging and electroencephalography. Anesthesiology *125*, 861–872.

30. Palanca, B.J.A., Avidan, M.S., and Mashour, G.A. (2017). Human neural correlates of sevoflurane-induced unconsciousness. Br. J. Anaesth. *119*, 573–582.

31. Jiang-Xie, L.F., Yin, L., Zhao, S., Prevosto, V., Han, B.X., Dzirasa, K., and Wang, F. (2019). A common neuroendocrine substrate for diverse general anesthetics and sleep. Neuron *102*, 1053–1065.e4.

32. Luo, T., and Leung, L.S. (2009). Basal forebrain histaminergic transmission modulates electroencephalographic activity and emergence from isoflurane anesthesia. Anesthesiology *111*, 725–733.

33. Weiner, D.M., Levey, A.I., Sunahara, R.K., Niznik, H.B., O'Dowd, B.F., Seeman, P., and Brann, M.R. (1991). D1 and D2 dopamine receptor mRNA in rat brain. Proc. Natl. Acad. Sci. USA *88*, 1859–1863.

34. Fremeau, R.T., Jr., Duncan, G.E., Fornaretto, M.G., Dearry, A., Gingrich, J.A., Breese, G.R., and Caron, M.G. (1991). Localization of D1 dopamine receptor mRNA in brain supports a role in cognitive, affective, and neuroendocrine aspects of dopaminergic neurotransmission. Proc. Natl. Acad. Sci. USA *88*, 3772–3776.

35. Zhang, Z., Wang, H.J., Wang, D.R., Qu, W.M., and Huang, Z.L. (2017). Red light at intensities above 10 lx alters sleep-wake behavior in mice. Light Sci. Appl. *6*, e16231.

36. Dong, H., Wang, J., Yang, Y.F., Shen, Y., Qu, W.M., and Huang, Z.L. (2019). Dorsal striatum dopamine levels fluctuate across the sleep-wake cycle and respond to salient stimuli in mice. Front. Neurosci. *13*, 242.

37. Lewis, L.D., Piantoni, G., Peterfreund, R.A., Eskandar, E.N., Harrell, P.G., Akeju, O., Aglio, L.S., Cash, S.S., Brown, E.N., Mukamel, E.A., and Purdon, P.L. (2018). A transient cortical state with sleep-like sensory responses precedes emergence from general anesthesia in humans. eLife *7*, e33250.

38. Xu, W., Wang, L., Yuan, X.S., Wang, T.X., Li, W.X., Qu, W.M., Hong, Z.Y., and Huang, Z.L. (2020). Sevoflurane depresses neurons in the medial parabrachial nucleus by potentiating postsynaptic $GABA_A$ receptors and background potassium channels. Neuropharmacology *181*, 108249.

39. Kelz, M.B., Sun, Y., Chen, J., Cheng Meng, Q., Moore, J.T., Veasey, S.C., Dixon, S., Thornton, M., Funato, H., and Yanagisawa, M. (2008). An essential role for orexins in emergence from general anesthesia. Proc. Natl. Acad. Sci. USA *105*, 1309–1314.

40. Yuan, X.S., Wang, L., Dong, H., Qu, W.M., Yang, S.R., Cherasse, Y., Lazarus, M., Schiffmann, S.N., d'Exaerde, A.K., Li, R.X., and Huang, Z.L. (2017). Striatal adenosine A_{2A} receptor neurons control active-period sleep via parvalbumin neurons in external globus pallidus. eLife *6*, e29055.

41. Alkire, M.T., Asher, C.D., Franciscus, A.M., and Hahn, E.L. (2009). Thalamic microinfusion of antibody to a voltage-gated potassium channel restores consciousness during anesthesia. Anesthesiology *110*, 766–773.

42. Alkire, M.T., McReynolds, J.R., Hahn, E.L., and Trivedi, A.N. (2007). Thalamic microinjection of nicotine reverses sevoflurane-induced loss of righting reflex in the rat. Anesthesiology *107*, 264–272.

43. Solt, K., Cotten, J.F., Cimenser, A., Wong, K.F., Chemali, J.J., and Brown, E.N. (2011). Methylphenidate actively induces emergence from general anesthesia. Anesthesiology *115*, 791–803.

44. Huang, Z.L., Qu, W.M., Eguchi, N., Chen, J.F., Schwarzschild, M.A., Fredholm, B.B., Urade, Y., and Hayaishi, O. (2005). Adenosine A2A, but not A1, receptors mediate the arousal effect of caffeine. Nat. Neurosci. *8*, 858–859.

45. Hambrecht-Wiedbusch, V.S., Li, D., and Mashour, G.A. (2017). Paradoxical emergence: administration of subanesthetic ketamine during isoflurane anesthesia induces burst suppression but accelerates recovery. Anesthesiology *126*, 482–494.

46. Kenny, J.D., Westover, M.B., Ching, S., Brown, E.N., and Solt, K. (2014). Propofol and sevoflurane induce distinct burst suppression patterns in rats. Front. Syst. Neurosci. *8*, 237.

47. Yang, C., Zhang, L., Hao, H., Ran, M., Li, J., and Dong, H. (2019). Serotonergic neurons in the dorsal raphe nucleus mediate the arousal-promoting effect of orexin during isoflurane anesthesia in male rats. Neuropeptides *75*, 25–33.

48. Vazey, E.M., and Aston-Jones, G. (2014). Designer receptor manipulations reveal a role of the locus coeruleus noradrenergic system in isoflurane general anesthesia. Proc. Natl. Acad. Sci. USA *111*, 3859–3864.

STAR★METHODS

KEY RESOURCES TABLE

REAGENT or RESOURCE	SOURCE	IDENTIFIER
Antibodies		
Rabbit polyclonal anti-Fos	Millipore	Cat#ABE457; RRID: AB_2631318
Donkey AlexaFluor488 anti-rabbit	Jackson ImmunoResearch	Cat#711-545-152; RRID: AB_2313584
Bacterial and virus strains		
AAV2/9-hSyn-FLEX-GCaMP6f	Taitool Bioscience	Cat#S0227-9
AAV2/9-hSyn-DIO-hM3D(Gq)-mCherry	Taitool Bioscience	Cat#S0192-9
AAV2/9-hSyn-DIO-hM4D(Gi)-mCherry	Taitool Bioscience	Cat#S0193-9
AAV2/9-hEF1α-DIO-mCherry	Taitool Bioscience	Cat#S0197-9
AAV2/9-hEF1α-DIO-hChR2(H134R)-mCherry	Taitool Bioscience	Cat#S0170-9
Chemicals, peptides, and recombinant proteins		
Isoflurane	RWD Life Science	Cat#R510-22
Sevoflurane	AbbVie	N/A
Clozapine-N-oxide	LKT	Cat#C4759
DAPI Fluoromount-G	Southern Biotech	Cat# 0100-20
Experimental models: organisms/strains		
Mouse: B6.FVB(Cg)-Tg(Drd1a-Cre) EY266Gsat/Mmucd, GENSAT	[11]	N/A
Oligonucleotides		
D1R-Cre mouse primers	JAX stock	Primers as recommended
Software and algorithms		
SleepSign 3.0	Kissei Comtec	RRID: SCR_018200
Spike2 Software	Cambridge Electronic Design	RRID: SCR_000903
ImageJ	N/A	RRID: SCR_003070
pClamp 10.3	Molecular Devices	RRID: SCR_011323
GraphPad Prism 8.0	GraphPad Software	RRID: SCR_002798
SPSS 19.0	IBM	RRID: SCR_019096
Adobe Illustrator	Adobe Systems	RRID: SCR_010279
Adobe Photoshop	Adobe Systems	RRID: SCR_014199
MATLAB R2018a	MathWorks	RRID: SCR_001622
Other		
Anesthesia monitor	Royal Dutch Philips Electronics	Cat#IntelliVue MP20
Sevoflurane vaporizer	Beijing Aeonmed	Cat#VP 3000
microtome	Leica	Cat#CM1950
vibratome	Leica	Cat#VT1200S
pipette puller	Sutter	Cat#P-1000

RESOURCE AVAILABILITY

Lead contact

Further information and requests for resources and reagents should be directed to and will be fulfilled by the Lead Contact, Zhi-Li Huang (huangzl@fudan.edu.cn).

Materials availability

This study did not generate new unique reagents.

Data and code availability

The data and codes generated or analyzed during this study are available from the corresponding author upon reasonable request (Zhi-Li Huang, huangzl@fudan.edu.cn).

EXPERIMENTAL MODEL AND SUBJECT DETAILS

Mice

D1R-Cre mice ((B6.FVB(Cg)-Tg(Drd1a-Cre) EY266Gsat/Mmucd, GENSAT; donated by Jiang-Fan Chen) were group-housed in a soundproof room (22 ± 0.5°C, 55 ± 5% humidity, food and water *ad libitum*) with an automatic 12-h light/dark cycle (illumination intensity »100 lux, lights on at 07:00).[11,35] Adult male D1R-Cre mice (8–10 weeks old) weighting 22–28 g were used for all experiments. Behavioral experiments were performed during the daytime. Animals were randomly assigned to different treatment groups. All experimental procedures were approved by the Animal Care and Use Committee of Fudan University. All procedures were conducted in accordance with the Guidelines of the NIH (United States) regarding the care and use of animals.

METHOD DETAILS

Surgery

Mice were anesthetized with 1%–2% isoflurane and placed on a stereotaxic frame (RWD Life Science, China). A heating pad was used to keep the temperature of each mouse constant throughout the operation. After sterilizing with 75% ethanol, an incision was made in the skin and small craniotomy holes were made above the target regions. A total of 70 nL of virus containing recombinant AAV-DREADD, AAV-ChR2, or AAV-mCherry (Taitool Bioscience, China) was bilaterally injected into the NAc (anteroposterior [AP] = +1.2 mm, mediolateral [ML] = ± 1.0 mm, dorsoventral [DV] = −4.5 mm deep relative to bregma) via a glass pipette and an air-pressure-injector system. The AAV-GCaMP6f virus (Taitool Bioscience, China) was unilaterally delivered into the NAc. After 5 min of injection to each site, the glass pipette was left at the injection site for 10 min and was then slowly pulled out. Three weeks after AAV injections, optical fibers (125 μm outer diameter [OD] 0.37 numerical aperture [NA]; Newdoon, Shanghai, China) were inserted toward the target regions followed by EEG/EMG electrode implantation, as previously described.[11,22] For *in-vivo* fiber photometry recordings and optogenetic experiments, the optical fiber cannula was placed above the NAc (AP = +1.2 mm, ML = ± 1.0 mm, DV = −4.0 mm). Cannulas were secured to the skull with dental cement. After implantation, mice were allowed at least 1–2 weeks for recovery before experiments.

Fiber photometry recording

As previously described,[11,36] a laser beam was passed through a 488-nm laser (OBIS 488LS; Coherent), reflected by a dichroic mirror (MD498; Thorlabs), focused by an objective lens (Olympus), and then coupled to an optical commutator (Doric Lenses, Canada). The light between the commutator and the implanted optical fiber was guided by an optical fiber (Newton, China). The GCaMP6f fluorescent signal was bandpass-filtered (MF525-39, Thorlabs) and collected by a photomultiplier tube (R3896, Hamamatsu). The photomultiplier-tube current output was converted to voltage signals by an amplifier (C7319, Hamamatsu), which was then filtered through a low-pass filter (40 Hz cut-off; Brownlee 440). The photometry analog voltage signals were digitalized at 512 Hz and recorded by using a Power1401 digitizer and Spike2 version-7 software (CED, Cambridge, UK) with simultaneous EEG/EMG recordings. Mice were first placed in an acrylic glass chamber connected to a sevoflurane vaporizer (VP 300; Beijing Aeonmed, China). After habituation, sevoflurane (1%, 1.5%, or 2.0%) with 100% oxygen—or only oxygen, as a control—was administered on different days to establish dose-response relationships. Sevoflurane concentrations were monitored by an anesthesia monitor (IntelliVue MP20, Royal Dutch Philips Electronics, Netherlands) connected to the chamber. Following 20 min of baseline recording after adaption in the chamber, sevoflurane was continuously delivered for 20 min. The recording was continued for another 20 min after switching off the sevoflurane vapor. We recorded Ca^{2+} signals for 60 min (20 min before, during, and after the administration of sevoflurane with oxygen) and calculated the averaged ΔF/F values before, during, and after treatments.

We further analyzed the real-time activities of NAc^{D1R} neurons during the induction and emergence phases of 2% sevoflurane, from wakefulness to the LOC state or from LOC to the ROC state, as determined by EEG/EMG recordings.[31] We identified state transitions and aligned ΔF/F with a window of −180 s ~ +300 s before and after 2% sevoflurane being turned on or off.[37] The onset of LOC was defined as the transition from a low-amplitude, high-frequency EEG to a high-amplitude, low-frequency EEG, combined with

continuously-minimal muscle tone.[31,38] We calculated the Ca^{2+} signals in three consecutive time sections (from −180 to 300 s, 0 s was the time point of 2% sevoflurane turning on): −180 to 0 s (pre-anesthesia baseline); the early period of anesthesia before LOC (pre-LOC, from 0 s to LOC); and the initial period after LOC (post-LOC, from LOC to 300 s). Additionally, the onset of ROC was defined as the point with a low-amplitude, high-frequency EEG combined with an obvious increase in EMG activity.[21,31] We analyzed the Ca^{2+} signals in three consecutive time sections (from −180 to 300 s, 0 s was the time point of 2% sevoflurane turning off): −180 to 0 s (unconsciousness anesthesia baseline); pre-return of consciousness (pre-ROC, from 0 s to ROC); and the initial period after ROC (post-ROC, from ROC to 300 s). One mouse was excluded from the analysis due to a lack of reliable EEG/EMG signals.

MATLAB R2018a software (Mathworks, USA) was further used to analyze the photometry data exported from Spike2.[36] The photometry signal, F, was converted to $\Delta F/F = (F - F_{baseline})/F_{baseline}$, where $F_{baseline}$ was determined during the 20 min recording period before gas inhalation. For analyzing the real-time activity of NAc^{D1R} neurons during induction and emergence phases of 2% sevoflurane GA, we first identified each state transition and segmented the data based on the EEG/EMG recordings. The photometry signal, F, was converted to $\Delta F/F = (F - F_{baseline})/F_{baseline}$, where $F_{baseline}$ was the baseline fluorescence signal during the induction period (−180 to 0 s, pre-anesthesia baseline) or during the emergence period (−180 to 0 s, unconsciousness anesthesia baseline). Furthermore, we calculated the average Ca^{2+} signals at baseline and during each state.

Chemogenetic manipulations

All behavioral experiments were undertaken between 09:00–17:00 h, with at least a 3-d washout between experiments.[11] Before experiments, mice were placed in a cylindrical LORR chamber with 1.5 L/min flow of 100% oxygen for 90 min for habituation over two successive days. After habituation, mice were pretreated with normal saline or CNO (C4759, LKT, USA) 3 mg/kg (intraperitoneally, i.p.) for 1 h before sevoflurane inhalation. To determine the dose–response curve for LORR, sevoflurane was initially delivered at 1.0% and was increased in increments of 0.1% every 15 min to allow for equilibration of the mouse at each concentration with the anesthetic vapor.[39] The cylindrical chamber was rotated 180° at the end of each 15-min interval to test for the righting reflex. When a mouse was unable to turn itself prone onto four paws within 30 s, it was considered to exhibit LORR. Induction and emergence experiments were conducted as follows. Mice were given normal saline (i.p.) or CNO (3 mg/kg, i.p.) at 1 h before 2% sevoflurane induction. The chamber was rotated every 15 s to check for LORR. The time to induction was defined as the interval between the onset of sevoflurane to the time when the mouse failed to right itself for more than 30 s. Normal saline or CNO (3 mg/kg, i.p.) was also delivered at 1 h before emergence testing. Each mouse was anesthetized with 2% sevoflurane for 1 h and was placed in the prone position, after which the door of the chamber was slightly opened to let room air inside the chamber. Emergence was defined as the time from the cessation of sevoflurane to RORR with all four paws touching the flour. LORR or RORR was confirmed by a second trial in all experiments, as described previously.[22,39] Mouse temperature was maintained by placing a 37°C heating pad under the chamber during all experiments.

Optogenetic stimulation during burst suppression

After habituation in the acrylic glass chamber, a 5-min baseline EEG/EMG (in wakefulness) was recorded. Then, 2.5% sevoflurane was initially delivered with oxygen at 1–2 L/min for induction.[21] After induction, 2.0% sevoflurane was continuously delivered. After entering a constant and stable burst-suppression oscillation mode for at least 5 min, light-pulse trains (5-ms pulses at 10–30 Hz for 30 s) were applied during continuous deep sevoflurane through a laser stimulator (SEN-7103, Nihon Kohden, Japan).[21,24] Before experiments, the power intensity of the blue light was tested by a power meter (PM10, Coherent, USA) as previously described.[11,22,40] Sevoflurane vapor was turned off at 6 min after the laser was turned off and the mouse was then removed from the chamber. Each mouse was tested over 2–3 experimental trials, with a 2-d interval between each trial.[19,31]

Optogenetic manipulations during CSSGA

We also explored light-pulse trains (5-ms pulses at 10–30 Hz for 60 s) during CSSGA with lighter sevoflurane, according to a previous protocol.[19] Briefly, after 5 min of an awake EEG/EMG baseline recording, each mouse was placed in the chamber to inhale 2.5% sevoflurane for 20 min, followed by placing the mouse on its back in the center of the chamber. The sevoflurane concentration was then lowered to 1.4%. If the mouse showed any signs of RORR, the chamber concentration was increased by 0.1% increments until the mouse maintained LORR for 20 min consecutively at a constant concentration. Therefore, the sevoflurane concentration, ranging from 1.4%–1.7%, slightly varied depending on the behavior of each mouse, as previously described.[19,41–43] After the 20-min equilibration period, acute optical stimulation (5-ms pulses at 10–30 Hz for 60 s) was initiated while the mouse continued to inhale the same concentration of sevoflurane during phtostimulation. The sevoflurane vapor was turned off at 6 min after the laser was turned off and the mouse was then removed from the chamber. Arousal responses of each mouse during the 60 s photostimulation period were scored according to analysis of video recordings.

EEG/EMG analysis

All EEG/EMG signals during optogenetic experiments were recorded and analyzed by SleepSign software (Kissei Comtec, Japan).[11,22,44] EEG/EMG signals were amplified and filtered (EEG, 0.5–30 Hz; EMG, 20–200 Hz), and were then digitized at a sampling rate of 128 Hz. EEG power spectra were calculated for consecutive 4 s epochs within the frequency range of 0–25 Hz using fast-Fourier transformation. EEG frequency bands (delta, 0.5–4.0 Hz; theta, 4.0–10 Hz; alpha, 10–15 Hz; beta, 15–25 Hz) were based on previous studies and relative changes in total power were calculated.[20,21] For optogenetic experiments during burst-suppression

oscillations, EEG changes from 28 s epochs within 90 s before, during, and after acute optical stimulation were computed. For CSSGA experiments, EEG changes from 60 s epochs within 120 s before and during photostimulation were analyzed.

BSR is a widely adopted method for quantifying burst suppression. Raw EEG data recorded by SleepSign software were converted to text format for further analysis of BSR using MATLAB R2018a software. EEG signals were processed by using the Hilbert transform to calculate the instantaneous amplitude and a visually-based threshold was set in the transformed signal to segment burst and suppression states for each mouse, as demonstrated previously.[45,46] A binary series was applied for BSR calculation, with the value being 1 if the transformed signal of EEG was outside the defined threshold and being 0 if it was within the threshold. The minimum duration of burst and suppression periods was set to 0.5 s.[20,45,47] BSR was calculated as the percentage of suppression at 30 s before, during, or after photostimulation of NAc^{D1R} neurons.

Arousal scoring during CSSGA

Arousal responses under sevoflurane CSSGA during acute photostimulation of NAc^{D1R} neurons were scored according to video recordings by accessors who were blinded to the experiments and were determined by an adaptation of the methods of previous studies.[19,41–43] Spontaneous movements of the head, tail, and limbs were scored as one of three levels: absent (0), mild (1), or moderate (2) in intensity. Righting was scored as 0 if the mouse remained with LORR, and 2 if the mouse recovered its righting reflex during the 60 s acute photostimulation. Walking after RORR was scored as follows: 0 = no further movements; 1 = crawled without the abdomen off the chamber bottom; and 2 = walked with the abdomen off the chamber bottom. The total score for each mouse depended on the sum of all categories and was determined during the 60 s acute photostimulation. Posterior densities for probabilities of righting and walking for the ChR2 group and mCherry group during CSSGA were drawn from beta distributions. The differences in probabilities of these arousal responses were also derived from beta distributions, as previously described.[19]

Immunohistochemistry

Immunofluorescence was performed as described previously.[11,40] Briefly, mice were deeply anaesthetized and were then intracardially perfused with phosphate-buffered saline (PBS) followed by 4% paraformaldehyde (PFA) in 0.1 M phosphate buffer (PB). For c-Fos immunostaining, mice were pretreated with either vehicle or CNO (3 mg/kg) for 1 h before anesthesia. For fixation, brains were kept in 4% PFA for 6 h after removal. For cryoprotection, brains were successively placed in 10%, 20%, and 30% sucrose in PBS at 4°C until they sank to the bottom. Brain samples were sectioned into 30-μm-thick coronal slices via a freezing microtome (CM1950; Leica, Germany) after embedding and freezing. Brain slices were washed three times in PBS and were then incubated with primary antibody in PBST (containing 0.3% Triton X-100) for 48 h on an agitator at 4°C using anti-c-Fos (1:8000, ABE457, Millipore, USA) antibody. Next, slices were washed three times in PBS and incubated at room temperature for 2 h with a donkey-anti-rabbit Alexa488 secondary antibody (1:1000, 711-545-152, Jackson ImmunoResearch, USA) in PBST. Then, brain slices were washed three times in PBS, mounted on glass slides, and coverslipped using DAPI Fluoromount-G (Cat# 0100-20, Southern Biotech, USA). Finally, fluorescent images were captured by an Olympus microscope or Leica confocal system. Only data from mice in which the AAV infection and the location of the optical fiber were confirmed were included. In this study, 42 mice with poor AAV expression, misplaced optical fibers, and/or loose electrodes were excluded from further analysis.

In vitro electrophysiology

Electrophysiological experiments were performed as previously described.[10,11] Briefly, after AAV-DIO-hM3Dq/hM4Di/ChR2-mCherry injection for 3–4 weeks, D1R-Cre mice were anesthetized with pentobarbital sodium (50 mg/kg, i.p.) and then transcardially perfused with ice-cold high sucrose solution containing (in mM): 2.5 KCl, 1.25 NaH_2PO_4, 26 $NaHCO_3$, 10 Dextrose, 2 Na-pyruvate, 0.4 ascorbic acid, 3 $MgSO_4$ and 0.1 $CaCl_2$, 213 sucrose and bubbled with 95% O_2 and 5% CO_2. Coronal slices (300 μm) containing the NAc were prepared using a vibratome (Leica VT1200S). Slices were incubated at 32°C for 30 min in a continuously aerated holding chamber containing artificial cerebrospinal fluid (aCSF) (in mM): 126 NaCl, 26 $NaHCO_3$, 25 glucose, 2.5 KCl, 2 $CaCl_2$, 1.25 NaH_2PO_4 and 1.0 $MgSO_4$. Neurons were visualized using a BX51WI microscope (Olympus) with an infrared-sensitive CCD camera (OptiMOS), mCherry-expressing NAc^{D1R} neurons were visualized with a green LED. Recordings were made in the NAc using a MultiClamp 700B amplifier (Molecular Devices). Signals were acquired using a DigiData 1440A A/D converter (Molecular Devices) filtered at 2 kHz and digitized at 10 kHz. The pipettes (6-8 MΩ) for recording NAc^{D1R} neurons contained (in mM): 130 potassium gluconate, 10 KCl, 10 phosphocreatine, 4 ATP-Mg, 0.5 EGTA, 0.5 GTP-Na, and 10 HEPES (pH 7.3, 285–300 mOsm). Series resistance was monitored throughout the experiment, and changes more than 20% were discarded. Optogenetic stimulation was applied with wide-field blue illumination (5 ms) using a blue LED (470 nm,1–100 Hz). The power of the LED light was 3–5 mW (Thorlabs). Data were acquired and analyzed using pClamp 10.3 software (Molecular Devices).

QUANTIFICATION AND STATISTICAL ANALYSIS

All data are expressed as the mean ± SEM. Sample sizes were chosen based on similar experiments using chemogenetic and optogenetic methods.[20–22,48] All data underwent Shapiro-Wilk normality tests before analysis. Parametric tests and non-parametric tests

were used based on the results of the normality tests. Paired or unpaired two-tailed Student's t tests were chosen for comparisons between two groups. If the data were not normally distributed, Wilcoxon signed-rank tests or Mann-Whitney rank-sum tests were used for further analysis. One-way or two-way repeated-measures ANOVAs followed by Tukey or Sidak's post hoc comparison tests were used for multiple comparisons. Graph Pad Prism 8.0 (GraphPad Software, USA) and SPSS 19.0 software (IBM, USA) were used for statistical analyses. Statistical details of all experiments can be found in the figure legends. In all cases, $p < 0.05$ was considered statistically significant.